Hydraulic Modeling and Flood Risk Assessment in the Hola and Bura Basins, Kenya: HEC-RAS-Based Simulation of the March 2024 *El-Niño* Event

Joseph Tinga Janga[1,3*], Edward Masibayi[2], Sam Waweru[1], Richard Onchiri[3]

[1]Department of Disaster Management-Internal Peace Support Training Centre, National Defence University-Kenya, P.O. Box 24232-00502 Nairobi; [2]Department of Civil Engineering and Structural Engineering, Masinde Muliro University of Science and Technology, P.O. Box 190-50100, Kakamega; [3]Department of Building and Civil Engineering, Technical University of Mombasa, P.O. Box 90420 – 80100, Mombasa, Kenya

Corresponding author's email: jangajosephtinga@tum.ac.ke

Abstract

This study presents a comprehensive hydraulic modeling and flood risk assessment of the Hola and Bura basins in Tana River County, Kenya, using the HEC-RAS 6.7 software. The model simulated the March 2024 *El-Niño* flood event, a climate-induced extreme rainfall episode, using a two-dimensional (2D) approach to capture complex flow dynamics across floodplains. Coupled with hydrologic inputs from HEC-HMS, the simulation produced detailed flood inundation maps and depth classifications, delineating shallow (< 0.5 m), moderate (0.5–1.5 m), and deep (> 1.5 m) flood zones across a total inundated area of 197.0 km²—representing 39% of the modeled basin. The analysis revealed critical floodplain features such as relict meanders and paleochannels that significantly influenced lateral water spread, emphasizing the importance of preserving natural floodplain connectivity. Validation using Sentinel-1 SAR imagery confirmed strong agreement between observed and simulated flood extents. The present study also assessed the vulnerability of key infrastructure assets, including roads, schools, hospitals, boreholes, and electric transformers. Findings indicate that critical services were either directly inundated or rendered inaccessible due to surrounding flood conditions, with power installations and boreholes particularly at risk due to exposure to deep, high-velocity flows. Based on the spatial hazard classification and exposure overlay, the study proposes targeted design improvements including elevated road embankments, flood-resilient water supply systems, and raised platforms for public utilities. The results demonstrate the value of integrating hydrodynamic modeling with satellite data and infrastructure mapping for informed disaster preparedness, climate adaptation, and land-use planning in flood-prone regions of East Africa.

Key Words: *El-Niño*, HEC-RAS, Flood Inundation, Critical Infrastructure, 2D Hydraulic Modeling, Climate Risk, Tana River, Kenya

Introduction

Flooding is one of the most persistent and destructive natural hazards in East Africa, responsible for repeated cycles of displacement, economic disruption, environmental degradation, and human loss. The impacts are particularly severe in low-lying, riverine regions like Tana River County, Kenya, where the Hola and Bura basins are located. These areas are not only hydrologically dynamic but are also increasingly pressured by anthropogenic drivers such as unregulated urbanization, expansion of irrigated agriculture, and catchment degradation. The result is a heightened level of exposure and vulnerability to flood events, particularly among marginal communities and critical infrastructure systems (World Bank, 2020; UNDRR, 2022). Kenya's vulnerability to flood hazards has grown over recent decades, with climate variability and land-use changes

Published December 2025

significantly altering the hydrologic regime. Seasonal floods in arid and semi-arid lands (ASALs), which make up over 80% of Kenya's landmass, have been growing in frequency and severity (FAO, 2015). The Hola and Bura irrigation schemes—designed to harness the River Tana's flow for food production—are increasingly affected by unanticipated overbank flows and prolonged floodwater stagnation. These systems are often compromised by poor drainage design, sedimentation, and encroachment into natural flood corridors, which restrict lateral water dispersion during high-flow events (FAO, 2015). The situation is further compounded by limited technical capacity and institutional coordination at the county level, creating a critical need for integrated flood risk assessment tools that are both accurate and applicable in resource-limited settings.

A major climatic amplifier of flood extremes in East Africa is the *El-Niño*–Southern Oscillation (ENSO) phenomenon. During *El-Niño* episodes, warm sea surface temperature anomalies in the eastern Pacific significantly alter atmospheric circulation, enhancing convective activity and increasing rainfall across much of the region (Dilley et al., 2005). Historical records confirm the strong relationship between *El-Niño* and extreme precipitation in Kenya. The 1997–1998 *El-Niño*, for example, was among the most devastating, bringing rainfall anomalies exceeding 150% above the seasonal average (Few, 2003). The consequences included submerged farmland, washed-out infrastructure, and over one million people affected nationwide (Otieno & Anyah, 2013). Similar trends were observed during the 2015 *El-Niño* event, with basin-wide flooding in Uganda's Lake Kyoga and River Tana's lower reaches (Nyeko, 2021).

The most recent March 2024 *El-Niño* event echoed this legacy, producing heavy rainfall in short durations, high antecedent soil moisture, and significant river discharge, particularly in the River Tana catchment. In the Hola and Bura basins, the result was widespread inundation, severe damage to crops and irrigation infrastructure, temporary displacement of urban populations, and critical service disruptions. Unlike previous flood events, however, this episode occurred in a context of improved satellite monitoring and hydrological modeling tools, presenting an opportunity to rigorously analyze the flood event using high-resolution simulations and evidence-based frameworks. Given the increasing complexity of flood risks—driven by both climatic and socio-economic transformations—there is an urgent need for advanced hydraulic modeling frameworks that go beyond empirical assessments. Hydraulic models allow for the simulation of water movement across terrain surfaces, enabling detailed analysis of flood depth, velocity, and extent. Among the most widely used platforms for this purpose is HEC-RAS (Hydrologic Engineering Center's River Analysis System), developed by the U.S. Army Corps of Engineers in 2021. The software is capable of simulating one-dimensional (1D) and two-dimensional (2D) unsteady flow dynamics and is increasingly adopted in both academic and applied flood studies. While 1D models have historically dominated riverine flood analysis, they are often insufficient in floodplains with complex terrain features, where lateral flow, backwater effects, and floodplain connectivity significantly influence flood behavior. In such contexts, 2D hydraulic modeling is essential (Horritt & Battes, 2002). Two-dimensional modeling offers spatially distributed outputs across a terrain mesh, providing realistic flood spread dynamics that consider surface slope, barriers, and depressions. These capabilities are particularly relevant in the Hola and Bura basins, where meander belts, oxbow lakes, and anthropogenic features such as roads and irrigation canals alter flow paths during floods. This study therefore, adopted a coupled hydrologic-hydraulic modeling approach to simulate the March 2024 *El-Niño* flood event.

The primary objectives of this research are fourfold. First, to simulate the flood extent and depth of the March 2024 *El-Niño* event in the Hola and Bura basins using a high-resolution 2D HEC-RAS model. Second, to classify flood hazard

zones based on depth thresholds that relate to infrastructure sensitivity and human safety. Third, to assess the spatial exposure of critical infrastructure—including roads, educational facilities, health centres, boreholes, and power installations—to varying flood intensities. Fourth, to generate actionable recommendations for improving infrastructure resilience, land-use planning, and emergency preparedness based on spatial flood insights.

Materials and Methods

Study Area and Data Sources

The present study focuses on the Tana River Basin, the largest and most socio-economically significant river basin in Kenya, covering an approximate area of 95,000 km² (Onywere et al., 2011). Geographically, the basin extends from the high-elevation Aberdare Range and Mount Kenya in the upstream catchment, through expansive mid-basin floodplains, and terminates in a delta system that discharges into the Indian Ocean. The basin supports critical economic activities including hydroelectric power generation, large-scale irrigation schemes—most notably the Bura and Hola schemes—and extensive downstream agriculture and pastoralism that sustain millions of livelihoods (Figure 1). Climatically, the basin spans diverse ecological zones, ranging from humid montane regions in the upper catchment to semi-arid and arid lowlands downstream. Rainfall follows a bimodal pattern, with the long rains typically occurring from March to May and short rains from October to December, driven by the seasonal migration of the Intertropical Convergence Zone (ITCZ) and strongly modulated by the *El-Niño*–Southern Oscillation (ENSO) phenomenon (Nicholson, 2017). The mean annual rainfall exceeds 2,000 mm/year in the highlands but drops below 500 mm/year in the lower plains, resulting in pronounced runoff variability and recurring flood risks, especially during strong *El-Niño* years (citation?).

Published December 2025

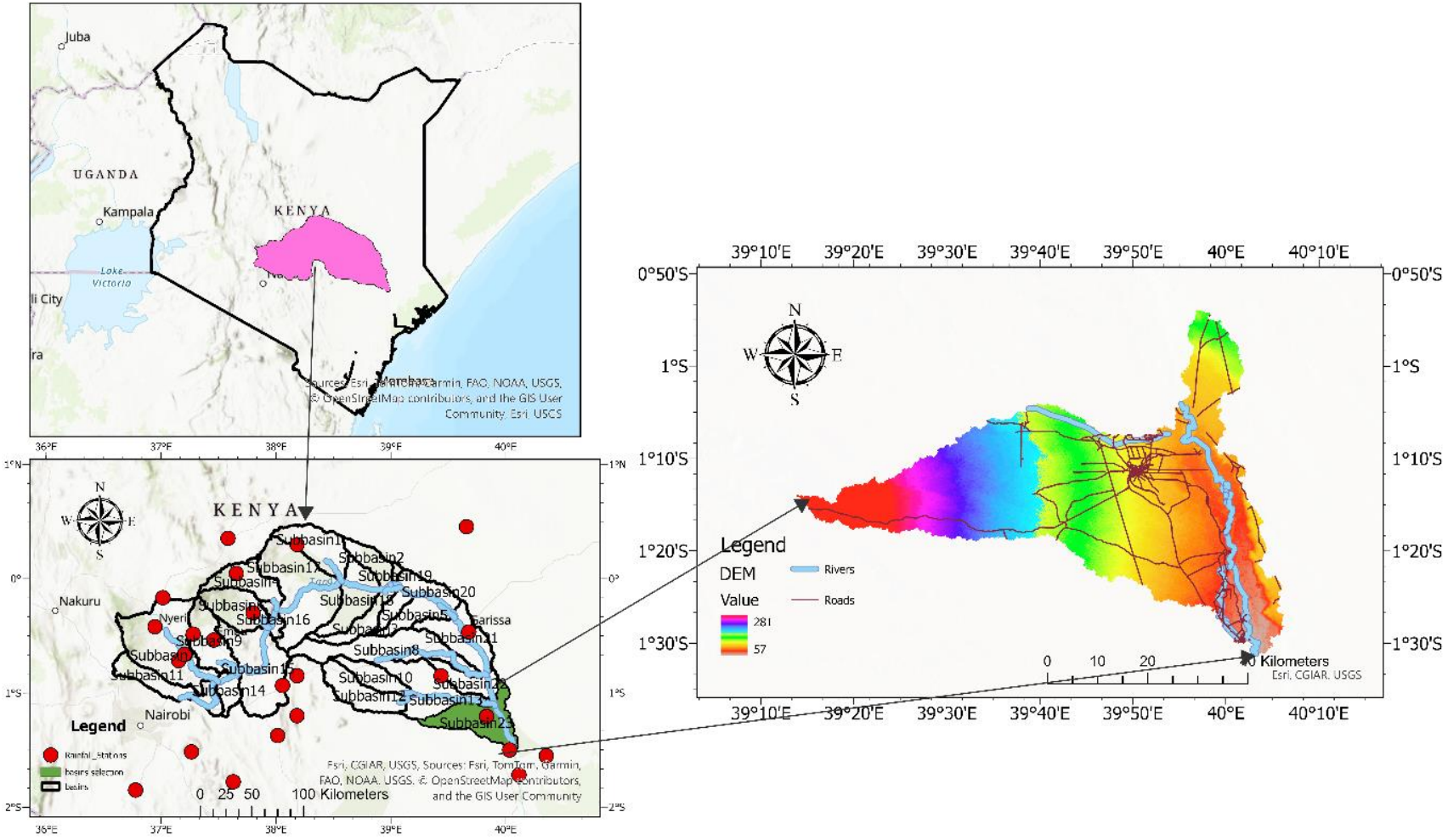

Figure 1. Location and data coverage of the Tana River Basin study area, including (a) the regional context within Kenya, (b) the delineated hydrological sub-basins with 30 rainfall gauge stations for HEC-HMS modeling, and (c) the zoomed-in DEM and river network of the Bura and Hola irrigation sub-basin used for detailed hydraulic modeling in HEC-RAS 2

Published December 2025

Data Collection and Compilation

To ensure an accurate representation of terrain, runoff generation, and river hydraulics, a comprehensive suite of datasets was compiled and systematically processed for hydrological and hydraulic modeling. Topographic information was derived from the Shuttle Radar Topography Mission (SRTM) digital elevation model (DEM) with a spatial resolution of 30 m (Farr et al., 2007; NASA JPL, n.d.). This DEM was used at two scales: for basin-wide hydrological modeling in HEC-HMS, the DEM facilitated delineation of the entire Tana River Basin upstream to the Bura and Hola schemes; for hydraulic modeling in HEC-RAS 2D, a refined sub-basin DEM was extracted to focus specifically on the Bura and Hola irrigation areas, ensuring high-resolution terrain representation for floodplain flow simulation (Figure 1c).

Daily rainfall records for March 2024, coinciding with a pronounced *El-Niño* event, were collected from 30 rain gauge stations distributed throughout the basin and its surroundings (Figure 1b). To address gaps in the observed data, satellite-based precipitation estimates, particularly the Climate Hazards Group InfraRed Precipitation with Station data (CHIRPS) and the Global Precipitation Measurement (GPM) IMERG products, were used for infilling and validation (Funk et al., 2015; Novella and Thiaw, 2013). This hybrid gauge–satellite dataset provided spatially continuous and temporally reliable rainfall input for the hydrological simulations. Daily discharge records from principal river gauging stations, provided by the Kenya Water Resources Authority (WRA), were used to calibrate and validate the HEC-HMS model, thereby improving the reliability of simulated flows feeding into the Bura and Hola sub-basin.

In addition, recent high-resolution Sentinel-2 imagery (~10 m) was classified to produce an up-to-date land use and land cover (LULC) map, identifying forests, crop lands, urban settlements, wetlands, and bare lands. This LULC data informed the assignment of Soil Conservation Service Curve Numbers (SCS-CN) for infiltration and runoff estimation in the hydrological model and guided the spatial allocation of Manning's roughness coefficients in the hydraulic model. Field-surveyed river cross-sections and detailed hydraulic infrastructure data—including irrigation canals, intake weirs, and levees—were incorporated into the HEC-RAS 2D model for the Bura and Hola irrigation sub-basin (Figure 1c). This level of detail enabled realistic simulation of channel flow, backwater effects, and overbank inundation within the irrigated areas.

Terrain Processing

Terrain processing provided the essential basis for both hydrological and hydraulic modeling in this study. All terrain data management and preprocessing tasks were performed using ArcGIS Pro 3.4 (Esri, 2023), while hydrological delineation and parameter extraction were conducted using HEC-HMS 4.12 (USACE, 2023a), and the hydraulic terrain preparation was handled directly within the Ras Mapper module of HEC-RAS 2D (USACE, 2023b). The Shuttle Radar Topography Mission (SRTM) 30 m digital elevation model (DEM) tiles covering the entire Tana River Basin were first acquired and mosaicked in ArcGIS Pro 3.4 to produce a seamless elevation surface for the study area (Farr et al., 2007; NASA JPL, n.d.). The mosaicked DEM was then clipped to the watershed boundary and reprojected into a uniform coordinate reference system consistent with other spatial datasets, such as rainfall gauge locations and land cover maps.

For hydrological modeling, terrain processing was performed within HEC-HMS version 4.12, which provides integrated tools for DEM conditioning, flow direction and flow accumulation grid generation, and automatic delineation of watersheds and stream networks. This ensured that sub-basin boundaries, drainage divides, and river reaches accurately represented the natural drainage system of the Tana River Basin up to the outlet at the Bura and Hola irrigation schemes. Watershed outlets,

confluence junctions, and routing reaches were defined in accordance with major hydrological control points and available gauging stations, providing a robust structure for rainfall-runoff simulation. Key hydrological descriptors required for parameterization were then derived within HEC-HMS, including sub-basin area, mean slope, longest flow path, and stream gradient. These attributes supported the estimation of time of concentration and unit hydrograph parameters critical for simulating runoff generation and flow timing.

For hydraulic modeling, detailed terrain preparation focused specifically on the Bura and Hola irrigation sub-basin. The modern Ras Mapper tool embedded within HEC-RAS 2D was used to process and refine the terrain model. The conditioned sub-basin DEM was imported into Ras Mapper, where a computational mesh was created that accurately captured the main river channel, surrounding floodplain topography, irrigation canal systems, and levee structures. This ensured high-resolution simulation of overbank flows, backwater effects, and local inundation patterns within the irrigated areas. This integrated terrain processing workflow—using ArcGIS Pro 3.4 for DEM mosaicking and projection, HEC-HMS 4.12 for watershed and stream network delineation, and Ras Mapper for hydraulic mesh generation—provided a consistent and high-fidelity topographic foundation for subsequent hydrological and hydraulic analyses. This robust foundation was crucial for accurately modeling runoff and floodplain dynamics during the March 2024 *El-Niño* event.

Hydrological Modeling Using HEC-HMS

The rainfall–runoff processes for the Tana River Basin were simulated using HEC-HMS version 4.12 (USACE, 2023a). This hydrological modeling framework included the development of a physically consistent basin model, interpolation and sub-basin allocation of rainfall inputs, specification of a design and event-based meteorological model, definition of control specifications, and execution of simulations to produce inflow hydrographs for subsequent hydraulic analysis. The rainfall-runoff transformation is carried out in HEC-HMS, which estimates flow hydrographs based on observed precipitation, soil characteristics, and basin geometry. These hydrographs are then input into HEC-RAS 6.7 to simulate flood routing and generate spatial outputs of inundation extent and depth. The hydraulic domain is constructed using a 30-meter Shuttle Radar Topography Mission (SRTM) Digital Elevation Model (DEM), with infrastructure layers—such as roads, boreholes, and transformer locations—integrated using GIS overlays. Validation is conducted using Sentinel-1 Synthetic Aperture Radar (SAR) imagery, allowing for an independent comparison of observed and simulated flood extent.

Basin Model

The Tana River Basin was subdivided into 23 hydrologically consistent sub-basins, delineated using the conditioned DEM and the extracted stream network. Sub-basins 1 to 22 represent upstream contributing catchments, while Sub-basin 23 specifically corresponds to the Bura and Hola irrigation sub-basin, modeled in greater spatial and hydraulic detail. For each sub-basin, hydrological parameters such as drainage area, average slope, longest flow path length, and stream gradient were derived within HEC-HMS using the terrain and LULC datasets. Soil Conservation Service Curve Numbers (SCS-CN) were assigned based on Sentinel-2 derived land use classes and hydrologic soil group data (USDA NRCS, 1986). Loss rates were estimated using the SCS-CN method, which is widely validated for tropical and semi-arid watersheds. Runoff transformation was performed using the SCS Unit Hydrograph method, appropriate for medium-to-large basins with moderate slopes (USACE, 2023a). Baseflow was simulated using the monthly constant baseflow method, which specifies a representative groundwater contribution for each calendar month, based on climatological estimates and historical low-flow records. Channel flow routing between sub-basin outlets and confluences was carried out using the

Muskingum routing method, a widely accepted approach for modeling flood wave translation and attenuation in natural river channels (Chow, 1959)

Rainfall Interpolation and Meteorological Model

Rainfall data for the March 2024 *El-Niño* event and synthetic design storms were obtained from 33 rain gauge stations distributed across the Tana River Basin and adjacent regions. Daily gauge observations were interpolated using the Inverse Distance Weighted (IDW) method within ArcGIS Pro 3.4 (Esri, 2023), producing spatially continuous rainfall surfaces. These rainfall rasters were then overlaid with the sub-basin polygons, and the mean daily rainfall depth was computed for each sub-basin to ensure that rainfall inputs matched the hydrological model structure. For the design storm scenarios, hyetographs representing 2-, 10-, 25-, 50-, and 100-year return periods were developed based on local Intensity–Duration–Frequency (IDF) curves and regional storm distribution patterns. The gauge weighting method within HEC-HMS was used to spatially allocate rainfall depths to the 23 sub-basins.

Control Specifications

The control specification in HEC-HMS was set to run at a daily time step, reflecting the temporal resolution of the available rainfall data and ensuring computational stability for a large basin scale. This daily resolution was appropriate for simulating both peak runoff and baseflow components over the extended time periods typical of basin-scale flood studies.

Model Execution

The integrated basin model, meteorological model, and control specifications were executed in HEC-HMS version 4.12. The model produced daily discharge hydrographs at each sub-basin outlet and key junctions along the Tana River system. The hydrograph generated for sub-basin 23 (Bura and Hola) served as the upstream boundary condition for detailed hydraulic simulation in HEC-RAS 2D. Model calibration and validation against historical discharge data from the Kenya Water Resources Authority ensured that the simulated runoff volumes, peak discharges, and baseflow components were consistent with observed river behavior, particularly during extreme events like the March 2024 *El-Niño* rainfall (USACE, 2023a).

Two-Dimensional Hydraulic Modeling

This study employed a two-dimensional (2D) hydraulic modeling approach to simulate unsteady floodplain and channel flows for the March 2024 *El-Niño* flood event. The modeling was implemented using the HEC-RAS 6.7 2D hydrodynamic module, developed by the U.S. Army Corps of Engineers (USACE, year?), which integrates advanced numerical solution schemes suitable for complex terrain and dynamic wetting–drying processes.

Governing Equations

The 2D hydraulic behavior was described by the depth-averaged shallow water equations (Saint-Venant equations) in conservative form:

Continuity:

$$\frac{\partial h}{\partial t}+\frac{\partial (hu)}{\partial x}+\frac{\partial (hv)}{\partial y}=0 \quad (1)$$

Momentum in x-direction:

$$\frac{\partial (hu)}{\partial t}+\frac{\partial (hu^2)}{\partial x}+\frac{\partial (uv)}{\partial y}=-gh\frac{\partial z}{\partial x}-\tau_{bx}+S_{fx} \quad (2)$$

Momentum in y-direction:

$$\frac{\partial (hv)}{\partial t}+\frac{\partial (huv)}{\partial x}+\frac{\partial (v^2)}{\partial y}=-gh\frac{\partial z}{\partial y}-\tau_{by}+S_{fy} \quad (3)$$

where h is water depth, u and v are depth-averaged velocity components in the x and y directions, z is the bed elevation, g is gravitational acceleration, and τ_{bx} and τ_{by} represent bed shear stresses in the respective

directions; S_{fx} and S_{fy} include additional source terms such as wind stress or external forces if relevant.

Computational Grid and Discretization

The study area was discretized using an unstructured computational mesh consisting of irregular cells that conform to the complex geometry of the river network and floodplain features. Mesh resolution was varied to balance accuracy and computational efficiency: finer cell sizes were applied within the main river channel, at hydraulic structures, and in high-gradient regions, while coarser cells covered extensive flat floodplain areas where detailed resolution was less critical. The governing equations were solved using a fully implicit finite volume method. For each cell, the general finite volume discretization is:

$$\frac{U_i^{n+1} - U_i^n}{\Delta t} V_i + \sum_{j=1}^{Nf} \left(F_{ij}^{n+1} \cdot \vec{n}_{ij}\right) L_{ij} = S_i^{n+1} V_i \quad (4)$$

where U_i is the vector of conserved variables (water depth and momentum components), $V_i$is the area of cell i, $F_{ij}$is the numerical flux across face j, $\vec{n}_{ij}$is the outward unit normal vector for face j, $L_{ij}$is the length of face j, and $S_i$represents source terms such as bed slope, friction, and external forces. The fully implicit formulation allows simultaneous solution of fluxes and source terms at the new time level, improving numerical stability especially in cases with rapid flood wave propagation and strong wetting–drying transitions.

Adaptive Time-Stepping and Solver Convergence

An adaptive time-stepping algorithm was implemented to dynamically adjust the simulation time step in response to local hydraulic conditions—such as high velocities, steep water surface slopes, or abrupt topographic variations—to ensure that hydraulic transients were adequately resolved. While the implicit scheme relaxes the strict Courant–Friedrichs–Lewy (CFL) constraint associated with explicit methods, the time step was automatically reduced in rapidly changing flow regions to maintain solution accuracy. The resulting nonlinear system of equations at each time step was solved iteratively using robust solvers. Stringent convergence criteria were enforced for mass and momentum conservation residuals, and the global mass balance was tracked throughout to ensure numerical consistency.

Wetting and Drying Treatment

Accurate floodplain modeling requires reliable representation of wetting and drying processes. HEC-RAS 2D implements a physically consistent wetting and drying algorithm that allows cells to transition seamlessly between dry and inundated states. A minimum depth threshold, typically 0.01–0.05 m, was used to suppress numerical instabilities in very shallow areas and ensure smooth propagation of the inundation front across diverse terrain.

Model Forcing, Execution, and Output

The hydraulic model was forced using hydrographs generated by the calibrated HEC-HMS rainfall–runoff model for the March 2024 *El-Nino* event. Simulations were executed to cover the full hydrograph duration, including the rising limb, peak flow, and recession phases, ensuring comprehensive capture of the flood wave dynamics. Key hydraulic outputs—such as water depth rasters, velocity vectors, and time-series water surface elevations—were recorded at user-defined intervals. These outputs were post-processed and integrated into a Geographic Information System (GIS) for detailed spatial analysis, inundation mapping, hazard classification, and risk assessment.

Validation and Quality Assurance

Model performance was validated through comparison of simulated hydrographs with observed discharge data at critical locations within the domain. Diagnostic checks included continuous monitoring of cumulative mass balance to detect numerical drift and inspection for nonphysical artifacts such as unrealistic velocity spikes or spurious oscillations. Where necessary, corrective actions—such as local mesh

refinement, solver parameter tuning, or adjustments to wetting and drying thresholds—were applied to maintain numerical robustness.

Boundary and Initial Conditions

Accurate specification of boundary and initial conditions is essential to ensure that the hydrodynamic simulations realistically reproduce the temporal and spatial dynamics of flood wave propagation within the study area (Brunner, 2020; USACE, 2021). The upstream inflow boundary conditions were defined using discharge hydrographs generated by the calibrated HEC-HMS rainfall–runoff model (USACE, 2023). These hydrographs captured the temporal distribution of flow during the March 2024 *El-Niño* flood event and were applied at key cross-sections along the main river channels and significant tributaries feeding into the Hola and Bura basins. At the downstream extent of the computational domain, stage–discharge relationships (rating curves) were applied where reliable observed gauge data were available, enabling realistic representation of backwater effects. In sections without empirical rating curves, a normal depth condition derived from local channel slope and cross-sectional geometry was specified to facilitate free outflow and minimize artificial flow reflections at the model boundary (Brunner, 2020).

Lateral domain boundaries were treated as no-flow (zero normal flow) wherever they coincided with natural topographic divides, ridgelines, or levees, ensuring that floodwater remained physically confined within the modeled floodplain (USACE, 2021). In areas where lateral inflow from smaller tributaries or distributed overland flow was significant but not directly represented by the upstream hydrographs, lateral inflow boundaries were prescribed based on excess rainfall runoff outputs from the HEC-HMS simulations (USACE, 2023). For each flood simulation, the river channels were initialized with a steady-state water surface profile representative of observed baseflow conditions immediately preceding the flood event (Brunner, 2020). Adjacent floodplain cells were initialized as dry, allowing the model to dynamically resolve the onset and progression of inundation in response to the advancing flood wave. This boundary and initial condition configuration ensured that the simulations conserved mass, maintained numerical stability, and realistically captured the flood wave's interaction with the complex channel and floodplain topography throughout the entire event duration.

Results and Discussion

The hydraulic modeling conducted using HEC-RAS 6.7 provided detailed insights into the behavior, extent, and impacts of flooding in the Hola and Bura basins during the extreme March 2024 *El-Niño* event. The use of 2D modeling techniques allowed for a realistic simulation of lateral flow distribution, dynamic floodplain connectivity, and the propagation of floodwaters across varied terrain features.

Flood Extent and Depth for the March 2024 *El-Niño* Event

Flood Extent

The simulated flood extent during the March 2024 *El-Niño* event spanned an estimated 197.0 km^2, which constitutes approximately 39% of the total modeled river basin area (Figure 2). This degree of inundation indicates a substantial hydrological response to the elevated precipitation intensities typically observed during *El-Niño* episodes. The extent and distribution of flooding were strongly influenced by the combination of saturated antecedent soil conditions and the temporal clustering of intense rainfall events, both of which are hallmarks of *El-Niño*-driven hydrometeorological patterns. The integrated HEC-HMS and HEC-RAS modeling system effectively captured these dynamics, translating hydrologic input into detailed spatial flood outputs.

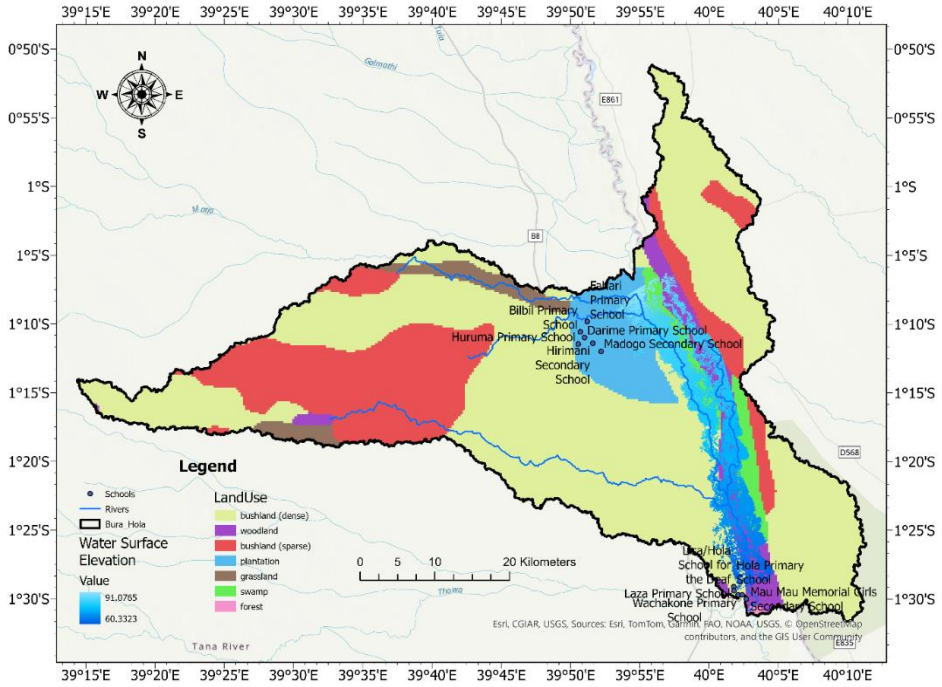

Figure 2. Simulated Maximum Flood Inundation Extent – March 2024 *El-Niño* Event

This simulation outcome aligns closely with historical and regional flood patterns reported during previous *El-Niño* events in East Africa. Otieno and Anyah (2013) highlighted that the 1997–98 *El-Niño* caused record-breaking rainfall in the region, leading to widespread flooding, infrastructure damage, and large-scale displacement. The same authors concluded that *El-Niño* significantly alters atmospheric circulation and increases convective activity over the region, resulting in rainfall surpluses of up to 150% above normal in some areas. Similarly, Nyeko (2021) used a combination of remote sensing and 2D hydraulic modeling to analyze the 2015 *El-Niño* floods in Uganda's Lake Kyoga Basin and found that between 35% and 40% of the basin's floodplain was inundated. This is comparable in magnitude and spatial pattern to the March 2024 flood event simulated in this present study, reinforcing the notion that basin-scale hydrologic responses under *El-Niño* conditions are both predictable and severe. A key insight from the spatial extent mapping was the activation of dormant floodplain features such as relict meander loops, oxbow lakes, abandoned channels, and seasonally active floodways. These features, typically dry or minimally active during normal hydrologic years, served as temporary storage and conveyance zones during the event. This behavior reflects the high sensitivity of floodplain morphology to extreme flow conditions. The model revealed that water spilled over main riverbanks and was redistributed through a network of natural depressions and paleochannels, facilitating rapid lateral spread across low-lying terrain.

This finding substantiates the work of Di Baldassarre et al. (2010), who emphasized the importance of preserving floodplain connectivity as a strategy for reducing downstream flood risk. Natural floodplains act as vital hydraulic buffers, temporarily detaining excess runoff and decreasing peak discharge rates. Their degradation—often through agricultural encroachment, settlement expansion, or infrastructure development—compromises this buffering capacity and leads to more concentrated flood impacts downstream. In the March 2024 event, areas where floodplain corridors remained intact exhibited wider but shallower inundation profiles, indicative of effective water distribution. In contrast, zones where development had restricted lateral flow

showed more abrupt transitions in flood depth and higher local water levels.

The spatial distribution of inundation also revealed land-use vulnerabilities. Extensive flooding was observed in agricultural regions, particularly along the southern and southeastern floodplain margins, where flat terrain and minimal structural protection enabled floodwaters to persist. Urban peripheries near Hola and Bura towns were affected as well, particularly in zones lacking adequate drainage infrastructure. These outcomes underscore the importance of integrating flood extent data into regional land-use planning and hazard zoning regulations.

Flood Depth Distribution

The flood depth distribution derived from the HEC-RAS 2D simulation was crucial for evaluating the severity and impacts of the March 2024 *El-Niño* flood event. The simulation categorized flood-affected areas into three hazard bands based on maximum water depth: deep flood zones (> 1.5 m), moderate flood zones (0.5 - 1.5 m), and shallow flood zones (< 0.5 m) (Figure 3). This stratification goes beyond mapping inundation extent alone and aligns with recommendations by Merz et al. (2007), who emphasized that flood depth is a key determinant of damage potential and human vulnerability. Such detailed classification enables more informed emergency response planning, infrastructure investment, and land-use management.

Deep flood zones, where water depths exceeded 1.5 m, accounted for about 23.7% of the total inundated area. These areas were primarily concentrated along the main river channel and hydrodynamically complex segments, such as pronounced meanders and concave banks. This pattern is consistent with findings by Horritt and Bates, (2002) and further supported by Di Baldassarre et al. (2009), who noted that channel curvature and bank geometry significantly influence flow energy and local depth increases during floods. In this simulation, notable deep-water accumulation zones included the southern fringe of Hola Town, where densely settled lowlands were severely impacted, and the intake structures of the Bura irrigation scheme, where channel constriction intensified inundation. Historical meander belts and paleochannels also stored large volumes of water, a phenomenon described by Schumann et al. (2018) in studies of relict fluvial landscapes. Deep floodwaters pose high risks to life, building integrity, and evacuation logistics, as highlighted by Jonkman and Kelman (2005), making accurate mapping and continuous monitoring vital for effective risk mitigation in riverine communities.

Moderate flood zones, with depths ranging from 0.5 to 1.5 m, represented the largest portion of the inundated area at 41.8%. These zones predominantly spanned extensive agricultural lands and peri-urban settlements. While less hydraulically forceful than deeper floods, moderate depths can persist for days, severely disrupting livelihoods and mobility. In agricultural settings, prolonged inundation submerged crops like maize and horticultural produce, causing near-total yield losses, echoing the conclusions of Wainwright et al., (2020) and corroborated by Dilley et al., (2005), who noted that moderate-depth floods often result in significant agricultural losses, especially during critical growing periods. In peri-urban areas, dwellings—many constructed without flood-resilient designs—experienced interior water damage, forcing evacuations and leading to asset loss. As argued by Few (2003), such zones should be prioritized for cost-effective flood-proofing measures, including raised building foundations, elevated roads, and community-scale levees.

Shallow flood zones, with depths under 0.5 m, accounted for 34.5% of the inundated area. Often underestimated in hazard assessments, shallow flooding mainly occurred along the outer edges of floodplains, on slightly elevated terrain, and near road networks and minor drainage routes. Despite lower water depths, these areas significantly disrupted transportation and accessibility for pedestrians and light vehicles, particularly where drainage systems were insufficient—an issue documented by Douglas et

al. (2008) in studies of urban floods in developing contexts. Consistent with Kefi et al. (2019), even shallow depths on roads cause delays, accidents, and economic losses due to restricted mobility. Moreover, shallow flood zones often serve as pathways directing water to deeper basins, playing a key role in the hydraulic connectivity of the floodplain, as noted by Neal et al. (2012). Mapping these pathways supports more effective flood routing, flow bottleneck identification, and informs strategic placement of structural interventions like culverts and diversion channels.

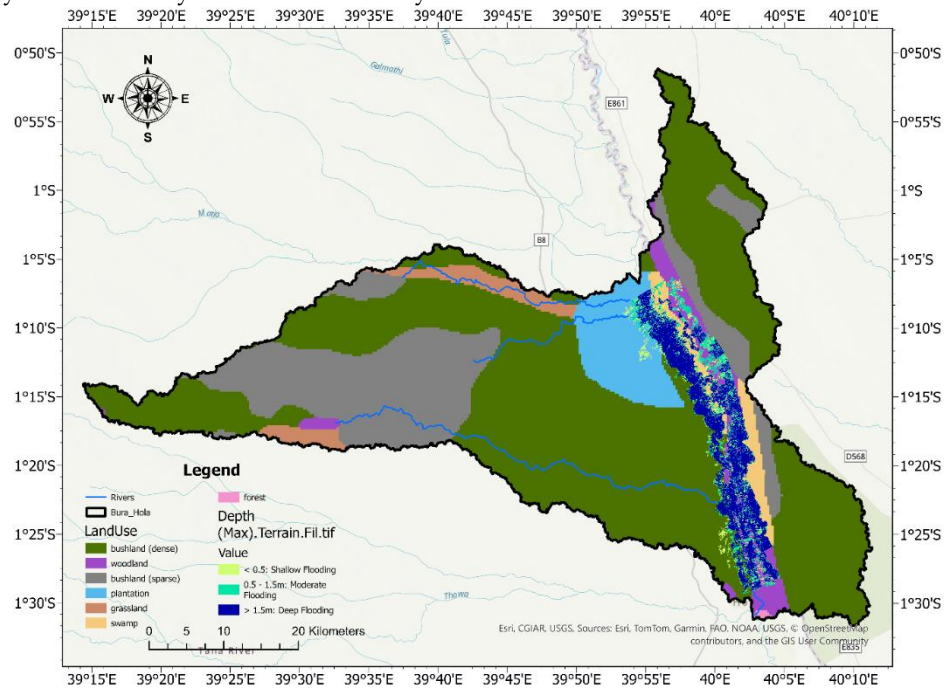

Figure 3. Simulated flood depth distribution of the Tana River Basin in Kenya

Agricultural and Urban Impacts

The March 2024 *El-Niño* flood event had significant implications for both agricultural production and urban settlements within the Hola and Bura basins. The simulation results and field observations indicated that agricultural fields near Hola were among the most severely impacted zones, particularly those situated on the southern floodplain adjacent to the river. These areas, dominated by maize and horticultural crops, were inundated with floodwaters of varying depths for prolonged periods. The combination of saturated soils and stagnant water exceeded the tolerance thresholds for most common crops. Notably, the persistence of floodwater for more than 48 hours in several fields likely resulted in complete crop failure, especially where water depths surpassed 0.8 m—a condition known to cause irreversible root damage and plant suffocation (Nicholson, 2017).

This scenario mirrors findings by Wainwright et al., (2020), whose hydrological modeling in Ethiopia under similar *El-Niño* conditions demonstrated that crop mortality sharply increases when submerged beyond two days, particularly for maize and vegetable crops during the growth or pre-harvest phase. In the Hola basin, such prolonged flooding not only threatens local food security but also disrupts the economic stability of smallholder farmers who rely on seasonal yields for both consumption and income generation. Furthermore, the inundation of irrigated plots within the Bura Irrigation Scheme may have damaged infrastructure such as canals, intakes, and farm access routes, potentially affecting future planting cycles and increasing the need for costly repairs.

Urban impacts were also significant, though more localized in comparison. The peripheral zones of Hola and Bura towns experienced shallow to moderate flooding, largely because of runoff accumulation, poor drainage, and floodwater intrusion from nearby river channels. Residential areas, particularly those lacking formal infrastructure or constructed in low-lying zones, faced temporary but severe challenges. These included property damage, flooded homes, and interruption of daily activities, with some areas reporting localized displacement and loss of household assets.

This vulnerability of urban peripheries is consistent with the analysis by Muthoni and Mwangi (2018), who found that even low-depth flooding (< 1 m) can critically affect informal settlements in Kenya. The same authors emphasized that limited drainage capacity, lack of flood-resilient construction, and socio-economic fragility make these communities highly susceptible to disruption. In the case of Hola and Bura, many of the affected households lacked the resources to implement protective measures such as sandbag barriers or elevated foundations. The result was not only material loss but also heightened health risks from stagnant water, blocked latrines, and restricted access to clean water and medical services.

Model Validation and Reliability

Overall, the comparison between SAR-based flood extent imagery with model-generated flood maps revealed strong spatial correlation between simulated and observed flood extents, particularly in the low-lying floodplains near Hola Town and along the main river corridor. The flood boundaries derived from the SAR imagery largely coincided with the predicted inundation footprint produced by the HEC-RAS 2D model, reinforcing the accuracy of the simulation in capturing the extent of overbank flow and lateral flood spread. This validation approach is consistent with best practices recommended by Schumann et al., (2009), who emphasized the utility of satellite-based flood imagery—especially SAR data—in data-scarce environments where field-based flood observations are limited or delayed. The advantage of using SAR is its ability to detect surface water in cloud-covered or turbid conditions, which are common during flood events (Schumann et al., 2009). Furthermore, Sentinel-1 provides repeat coverage at high spatial resolution (10–20 m), enabling detailed detection of inundation patterns in both urban and rural areas. The consistency between model and observation supports the suitability of the modeling framework, input parameters, and hydrologic boundary conditions applied during the simulation.

Despite the generally good agreement, some discrepancies were observed, particularly in areas adjacent to artificially elevated infrastructure, such as embankments and roadways. In several instances, the model appeared to over predict flood extents beyond the actual observed boundaries. This was most evident where roads had been elevated or reinforced locally but were not accurately captured in the Digital Elevation Model (DEM) used for terrain processing. These overestimations are attributed to the limitations of the Shuttle Radar Topography Mission (SRTM) DEM, which served as the foundational elevation input for the hydraulic model. As noted by Wood et al., (2016), while the 30-m resolution SRTM dataset is generally sufficient for regional-scale hydrologic modeling, it lacks the granularity to resolve small-scale elevation variations such as culverts, levees, curbs, and roadside berms. These features can significantly influence localized flow paths and inundation depth, particularly in semi-urban or infrastructure-dense environments. The vertical smoothing inherent in SRTM processing can also flatten embankments and artificially depress road surfaces, leading to inaccurate representations of flow barriers or storage areas in the model.

Impact on Critical Infrastructure

Road Networks

The analysis revealed that approximately 12.4 km long of the primary Hola–Garsen road was inundated at the flood's peak, predominantly affecting sections adjacent to the River Tana and within flood-prone low-lying zones. Visual assessment of the road network from the flood map (Figure 4) indicates that the most affected segments were concentrated east and southeast of Hola Town, particularly where the road crosses or runs parallel to deep flooding zones (>1.5 m depth, marked in dark blue; Figure 4). Inundation depths along the Hola–Garsen road varied from 0.3 m in shallow flood zones (light green) to over 1.5 m in deeper flood zones, especially in areas lacking raised embankments or adequate culverts. These depths rendered the road impassable for both light and heavy vehicles during the flood peak, effectively severing connectivity between Hola and downstream settlements toward Garsen.

Secondary roads and rural tracks also experienced significant disruption. The same figure shows multiple secondary roads intersecting moderate (0.5– 1.5 m depth) and deep flooding zones, especially those radiating southeast and south of Hola. Roads leading toward the east and northeast of Hola appeared less affected, mostly skirting shallow flood zones or elevated terrain. However, rural tracks in the southern and southwestern sectors were notably inundated, isolating peripheral farming communities. The functional isolation of rural communities—due to the disruption of both primary and secondary roads—had cascading impacts on access to emergency services, markets, health facilities, and urban centres. Areas within the southern floodplain and the eastern corridor along the River Tana were most vulnerable to isolation, as reflected by the density of roads overlapping deep flooding zones in these sectors. This spatial pattern highlights the urgent need for climate-resilient road infrastructure, including raised road embankments, installation of additional drainage culverts, and consideration of flood pathways in future road alignments. Priority interventions should focus on the Hola–Garsen corridor's low-lying segments and secondary road crossings within moderate to deep flood zones, as identified on the flood risk map.

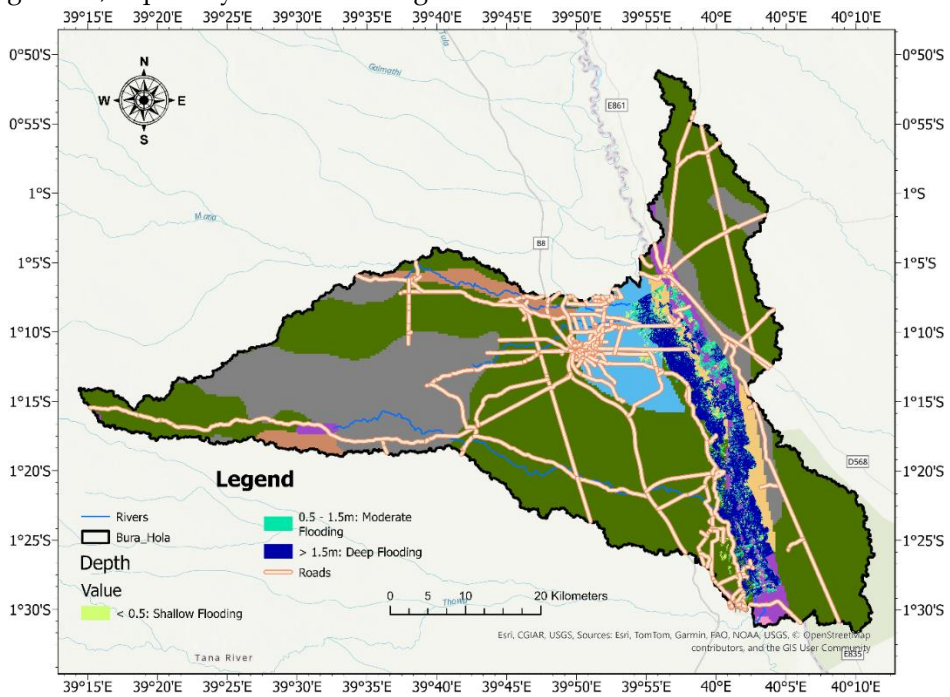

Figure 4. Map showing flood depth zones and road network in the Bura-Hola area, indicating areas of shallow, moderate, and deep flooding affecting road infrastructure

Published December 2025

Educational Facilities

Spatial analysis of the flood impact map (Figure 5) indicates that at least 9 schools were located within flood-affected areas, intersecting shallow, moderate, and deep flooding zones. These include 5 primary schools (Huruma, Bilbil, Fahari, Darime, Madogo) and 2 secondary schools (Hirimani and Mau Mau Memorial), along with other educational facilities situated near the eastern floodplain of the River Tana. The majority of schools exposed to flooding were located along the eastern corridor of the Bura_Hola region, where deep flooding zones (> 1.5 *m*, marked in dark blue; Figure 5) were concentrated. The primary schools of Huruma, Bilbil, and Fahari were within or adjacent to moderate to deep flooding zones, resulting in inundation depths estimated between 0.6 and 1.4 m at the peak of flooding. Ground floors, access roads, playgrounds, and sanitation blocks were submerged, compromising both the structural integrity and safe operation of these facilities.

Notably, Hirimani Secondary School and Madogo Primary School were also exposed to floodwaters, though their locations on the map suggest partial inundation within moderate depth zones (0.5– 1.5 *m*, light blue; Figure 5) rather than the deepest flood areas. The Mau Mau Memorial Secondary School and Laza Primary School, located further south, were situated near the boundary of shallow to moderate flooding zones, facing localized but still impactful flood exposure. The flooding necessitated extended school closures due to a combination of factors: water damage to classrooms, collapsed pit latrines, contamination of water supplies, and impassable access routes for staff and students. The closure of these educational facilities disrupted learning for thousands of children in the floodplain, with long-term implications for education continuity and community resilience.

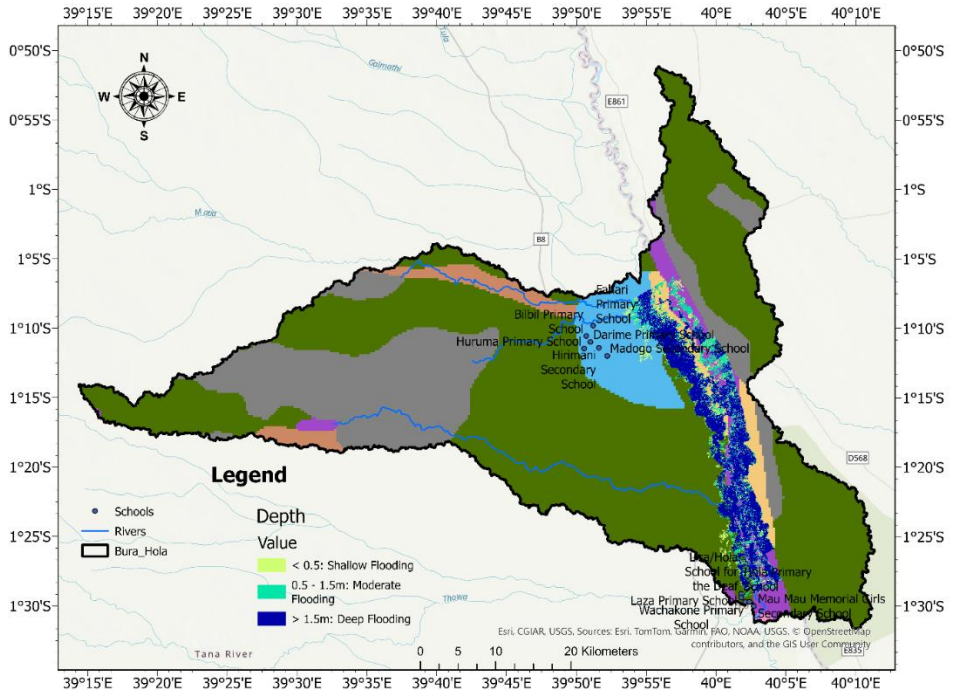

Figure 5. Map showing the distribution of schools within the Bura Hola region overlaid on flood depth zones, indicating varying levels of flood exposure for educational facilities.

Health Facilities

Spatial analysis of the flood impact map (Figure 6) indicates that two key health centres—Bura sub-County Hospital and Hola County Referral Hospital—remained physically above critical

Published December 2025

flood depths, situated within areas experiencing shallow flooding (< 0.5 m, marked in light green; Figure 6). Although the hospital buildings were out of direct inundation from deeper floodwaters, their functional accessibility was severely compromised due to surrounding road and terrain flooding. The same figure shows that both facilities were effectively encircled by areas of moderate (0.5– 1.5 m) and deep flooding (> 1.5 m) along primary access routes. In particular, the main roads leading east and southeast from Hola, and southwest from Bura, intersected deep flooding zones (marked in dark blue), cutting off vehicular passage for ambulances, staff, and patients. Consequently, despite the hospitals' structural integrity, emergency healthcare delivery was significantly disrupted during the peak flood period, as patients from isolated rural areas could not reach the facilities. This spatial pattern underscores the critical dependency of healthcare resilience not only on facility elevation but also on the flood vulnerability of access roads and transport corridors. The limited accessibility of these key health centres posed serious public health risks by delaying treatment of injuries, waterborne diseases, and other acute conditions during the flood emergency.

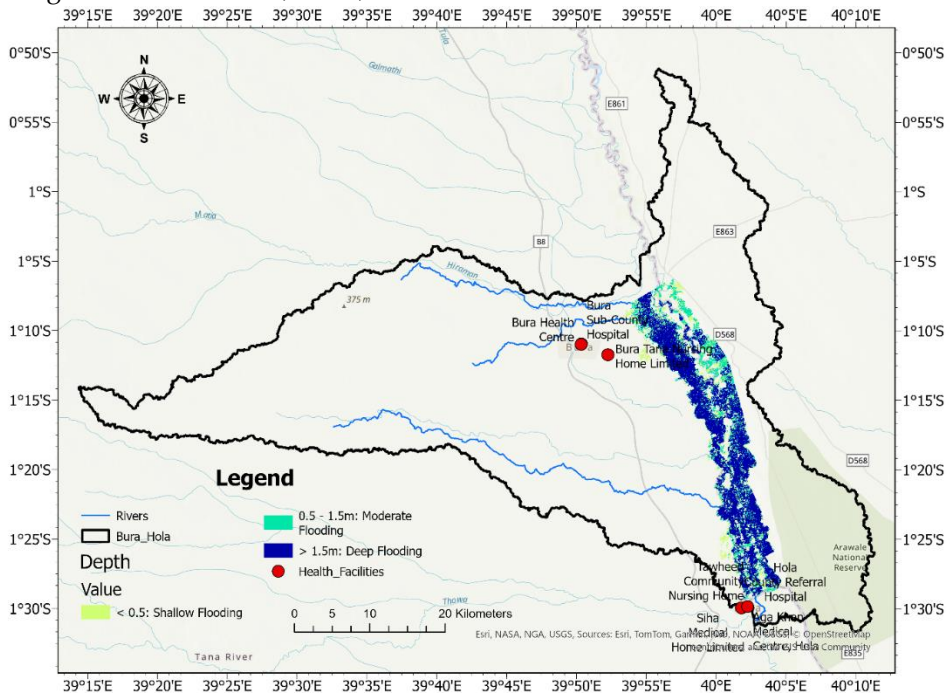

Figure 6. Map showing the location of health facilities in Bura and Hola relative to flood depth zones and access routes.

Water Supply Systems -Boreholes

Results revealed that 8 operational boreholes across the Hola and Bura sub-basins were located within high-risk flood zones (Figure 7). These areas experienced maximum inundation depths exceeding 0.5 m, with some locations submerged for several consecutive days. These boreholes serve as vital sources of potable water for rural and peri-urban populations, many of whom lack access to piped or treated water infrastructure. The extended submersion of these boreholes during the flood significantly increased the risk of contamination by flood-borne pollutants. In the Hola sub-basin, 4 boreholes were identified in the villages of Makere, Kipini South, Garsen East, and Mororo. The remaining 4 were located in the Bura sub-basin, specifically in Bura Tana South, Chewele, Kinakomba, and Mnazini. All 8 boreholes were situated in or near active floodplains and experienced flood depths ranging from 0.6 to 1.3 m at peak inundation. These conditions pose a direct threat to water safety and infrastructure integrity.

Published December 2025

Floodwaters in these areas typically carry organic waste, sediment, agricultural runoff, and chemical contaminants from surrounding infrastructure and farmland. When borehole heads and casings are submerged—especially in the absence of protective sealing—there is a high risk that these contaminants will infiltrate the groundwater system. This creates a dangerous pathway for the transmission of waterborne diseases such as cholera, typhoid, dysentery, and hepatitis A, particularly among displaced populations and communities with inadequate sanitation systems. Furthermore, many of the affected boreholes lack essential protective features such as concrete aprons, elevated wellheads, or sealed pump assemblies, leaving them highly vulnerable during extreme flood events. Post-flood assessments confirmed that several boreholes were rendered inoperable due to siltation, mechanical damage, or microbial contamination. These failures necessitated costly repairs and emergency water trucking services to ensure continued water access.

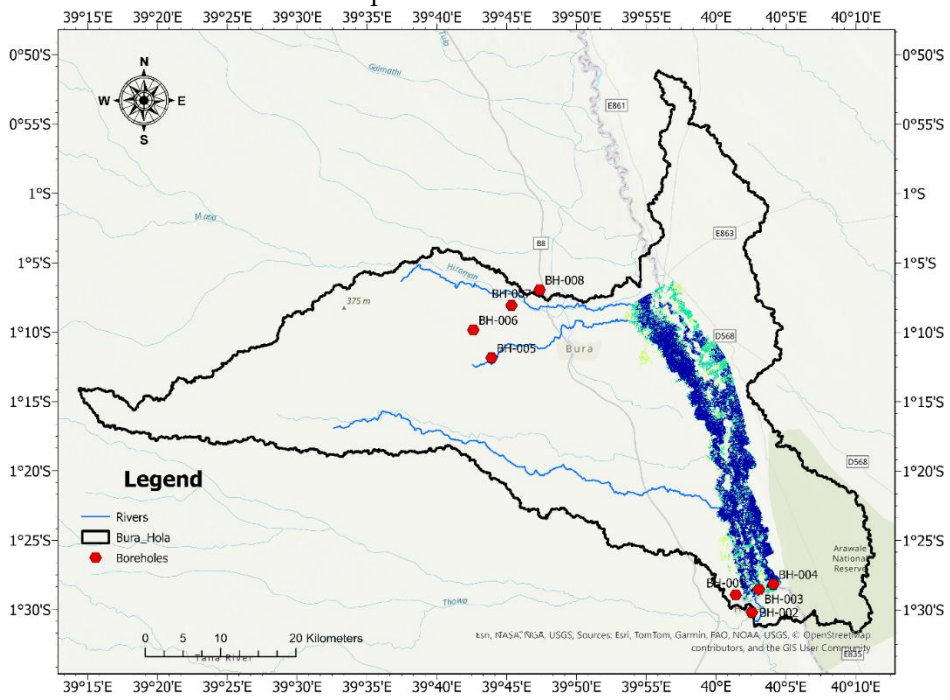

Figure 7. Overlay of Borehole Locations and Simulated Flood Inundation Extent in the Hola and Bura Sub-basins

Figure 7 visually overlays the locations of boreholes (BH-001 to BH-008) with simulated flood inundation zones, depicted in colour gradients representing different depth ranges ($< 0.5\ m, 0.5–1.5\ m, > 1.5\ m$). This spatial analysis supports the evaluation of each borehole's exposure level and informs site-specific risk mitigation strategies. In the Hola sub-basin, boreholes BH-001 (Makere), BH-002 (Kipini South), BH-003 (Garsen East), and BH-004 (Mororo) were clustered in the southern floodplain, where the figure shows dense and extensive inundation. BH-001 and BH-003 were particularly vulnerable, located within areas of deep flooding that exceeded 1.1 m. BH-002 and BH-004 were surrounded by moderate flood zones, exposing them to contamination risks. The proximity of these boreholes to the River Tana's core floodplain increases their vulnerability and signals a critical need for infrastructure fortification or relocation.

In the Bura sub-basin, boreholes BH-005 (Bura Tana South), BH-006 (Chewele), BH-007 (Kinakomba), and BH-008 (Mnazini) were more spatially distributed, mostly along smaller tributaries or flood channels. BH-005 and BH-006 were partially submerged, indicating potential for microbial infiltration. BH-007, located upstream but still near a smaller flooded stream,

Published December 2025

experienced the highest flood depth (1.3 m) among Bura boreholes. BH-008, situated closer to the basin's edge, lies within light flood zones and is classified as moderate-risk. The flood exposure map (Figure 7) reinforces the results of the hazard analysis by clearly illustrating that boreholes in the Hola sub-basin are situated within the most heavily inundated areas. This finding underscores the urgent need for adaptive interventions such as elevating wellheads, reinforcing borehole structures, and, where necessary, relocating installations that face repeated or severe flood exposure. Although the Bura sub-basin experienced less extensive inundation overall, boreholes in this area remain vulnerable to localized flooding, compromised foundations, and surface water infiltration. The figure demonstrates the critical importance of spatial risk overlays as a strategic tool for identifying infrastructure at risk and for prioritizing flood-resilient upgrades across both sub-basins.

Electric Power Infrastructure

Results identified two critical electric transformer installations located within high-velocity flood zones in the Hola and Bura sub-basins (Table 1 and Figure 8). These zones experienced surface flow speeds exceeding 2 m/sec, exposing the transformers to intense hydrodynamic forces. Positioned in low-lying and hydraulically active areas, these installations are vital components of the regional power distribution network, supplying electricity to both residential communities and essential public service facilities. During the peak flood event, these transformers were not only subjected to direct inundation but also to erosion and scouring from fast-moving floodwaters—conditions that significantly elevate the risk of structural failure and power disruption. While the overhead transmission lines remained largely unaffected by inundation or wind damage, their supporting structures—primarily concrete and wooden poles—were compromised by sustained soil saturation. Extended waterlogging reduces soil strength and destabilizes pole foundations, increasing the likelihood of tilting or collapse. In several cases, localized washouts were observed around pole bases, underscoring the urgency for structural reinforcement and post-flood inspections. The implications of such vulnerabilities are significant. Electric power infrastructure is a backbone of disaster resilience, especially during flood events when continuous electricity is essential for operating health facilities, maintaining water supply systems, supporting early warning mechanisms, and enabling emergency communications. In rural areas of Bura, temporary power outages were reported during the flood's peak, directly affecting medical response capabilities and isolating some communities from critical services.

Table 1. Electric Power Infrastructure in Hola and Bura sub-Basins

Asset ID	Sub-basin	Location	Latitude	Longitude	Flood Velocity (m/s)	Flood Depth (m)	Risk Level
TR-001	Hola	Hola Town (Central)	-1.4850	40.0350	2.3	1.1	High
TR-002	Bura	Chewele Transformer	-1.1600	39.7150	2.1	0.9	High

Transformer TR-001(Table 1), located in Hola Town near the Tana River floodplain, is situated within a densely built urban environment where it plays a critical role in supplying power to essential public services. During the March 2024 flood event, this installation was directly impacted by floodwaters and high-velocity surface flows, resulting in base inundation and visible erosion of the surrounding ground. Its strategic location near key infrastructure—

Published December 2025

including health facilities, water supply systems, and emergency coordination centres—means that any failure at this site would have wide-reaching implications for disaster response and community well-being. In comparison, transformer TR-002, located in Chewele Village within the Bura sub-basin, experienced less severe flooding but was still affected by high-velocity runoff and persistent soil saturation around its foundation. Although the transformer remained functional during the event, the hydrological stress placed on its structural stability elevated the risk of future failure. This concern is particularly pronounced in rural settings like Bura, where backup energy systems are limited and power restoration following outages tends to be slow and resource intensive.

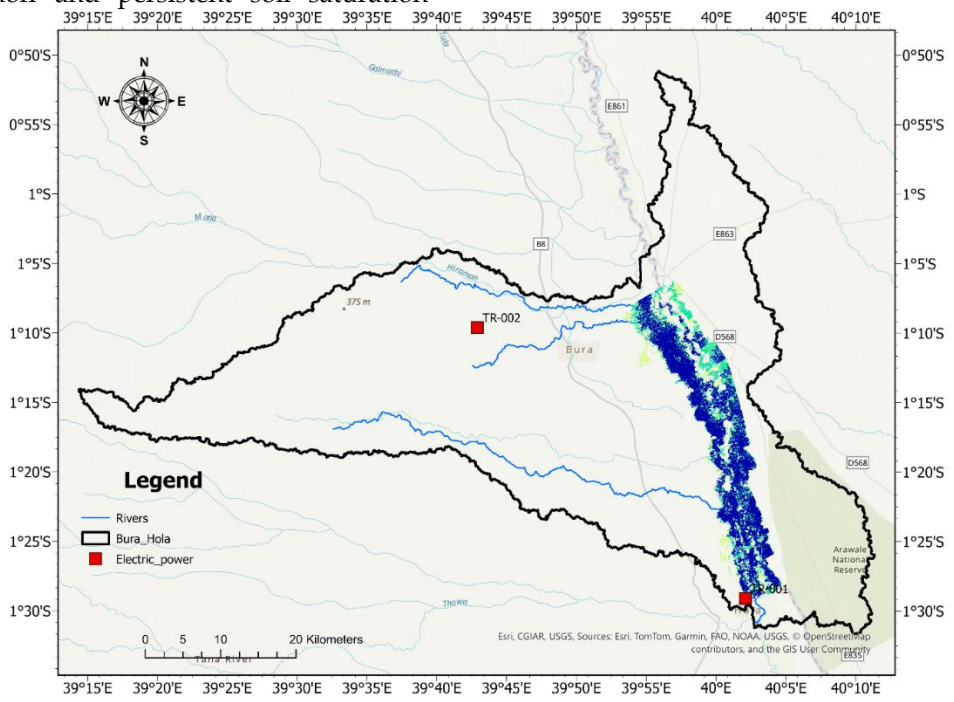

Figure 8. Electric Power Infrastructure Exposure to Simulated Flood Inundation in the Hola and Bura Sub-basins (March 2024 Event)

This Figure 8 illustrates the spatial distribution of key electric power infrastructure in relation to simulated flood inundation zones. Transformer locations (TR-001 and TR-002) are shown as red squares, overlaid on color-coded flood zones representing varying depths. TR-001, near the Tana River in Hola, lies within a high-depth flood area and faces significant inundation and erosion risk. TR-002, in Chewele Village, Bura sub-basin, is situated near a tributary with moderate exposure to high-velocity flows. Figure 8 underscores the vulnerability of power systems to climate-driven flood hazards and highlights priority areas for resilience planning.

Conclusion

The modeling results revealed that approximately 197.0 km² (39%) of the analyzed area, was inundated during the flood event, with depths ranging from shallow overbank flooding to deep channel overflow conditions. The results of the March 2024 *El-Niño* flood simulation carry significant implications for flood risk management, land-use planning, and climate resilience in the Hola and Bura basins, and more broadly across similar flood-prone regions in East Africa. Deep flood zones (> 1.5 m) represent areas of high hazard intensity and should be prioritized for evacuation planning, infrastructure floodproofing, and restrictive zoning regulations. Moderate flood zones (0.5–1.5 m), which accounted for the largest proportion of inundation in the simulation, warrant a combination of adaptive infrastructure design and risk-sensitive urban expansion

policies. Shallow flood zones (<0.5 m), though often overlooked in planning, can result in substantial functional and economic disruption, particularly in rural areas where road networks, footpaths, and drainage infrastructure are not flood resilient.

This study recommends all critical public facilities, particularly schools and health centres, should be constructed on elevated platforms or retrofitted with raised floor slabs and reinforced foundations to ensure continued functionality during flood events. Reliable access to safe drinking water must be safeguarded by flood-proofing borehole infrastructure. Roads and power systems in flood-prone corridors should be upgraded to enhance resilience to extreme hydrological events. Future hydraulic modeling and flood risk assessments should integrate detailed infrastructure data to better simulate the interaction between built structures and flood dynamics. Given the spatial overlap between school locations and flood risk zones, the findings highlight an urgent need for flood risk reduction measures targeting educational infrastructure. There is need for adoption of flood-resilient design standards in the area. This include installing raised borehole platforms, sealed protective casings, backflow prevention devices, and incorporating chlorination or point-of-use disinfection systems. There is need for targeted resilience measures for electric power assets in flood-prone areas. It is essential to institutionalize the outputs of hydraulic and flood risk modeling within county-level spatial planning, development controls, and disaster risk management frameworks.

Acknowledgement

The successful completion of this study, would not have been possible without the support, guidance, and encouragement of many individuals and institutions. We are deeply grateful to Masinde Muliro University of Science and Technology (MMUST) for providing the facilities and academic environment that enabled the successful execution of the hydraulic modeling and flood risk assessment. Special thanks are also extended to the Tana River County Government and the Kenya Meteorological Department for providing essential hydrological and meteorological data for the study area. We wish also to acknowledge the contributions of local stakeholders and community representatives in the Hola and Bura basins, whose insights and first-hand accounts of the March 2024 *El-Niño* event greatly enhanced the contextual understanding of the flood risks assessed in this study.

References

Brunner, G.W. (2020). *HEC-RAS River Analysis System Hydraulic Reference Manual* (Version 6.0) U.S. Army Corps of Engineers, Hydrologic Engineering Centre.

Chow, V.T. (1959). *Open-channel hydraulics*. McGraw-Hill.

Di Baldassarre, G., Schumann, G., & Bates, P.D. (2010). A technique for the calibration of hydraulic models using uncertain satellite observations of flood extent. *Journal of Hydrology,* 394(3–4): 357–367 https://doi.org/10.1016/j.jhydrol.2010.09.002

Dilley, M., Chen, R.S., Deichmann, U., Lerner-Lam, A.L., & Arnold, M. (2005). *Natural disaster hotspots: A global risk analysis*. World Bank Publications

Douglas, I., Alam, K., Maghenda, M., McDonnell, Y., McLean, L., & Campbell, J. (2008). Unjust waters: Climate change, flooding and the urban poor in Africa. *Environment and Urbanization*, 20(1):187–205. https://doi.org/10.1177/0956247808089156

Esri. (2023). *ArcGIS Pro 3.4* [Computer software]. Environmental Systems Research Institute.https://www.esri.com/en-us/arcgis/products/arcgis-pro/overview

FAO. (2015). *Irrigation in Africa in figures: AQUASTAT Survey – Kenya*. Food and Agriculture Organization of the United Nations, Rome. https://www.fao.org/aquastat/en/

Farr, T.G., Rosen, P.A., Caro, E., Crippen, R., Duren, R., Hensley, S., ... & Alsdorf, D. (2007). The Shuttle Radar Topography Mission. *Reviews of Geophysics:* 45(2) RG2004. https://doi.org/10.1029/2005RG000183

Few, R. (2003). Flooding, vulnerability and coping strategies: Local responses to a global threat. *Progress in Development Studies*, 3(1): 43–58 https://doi.org/10.1191/1464993403ps049ra

Funk, C., Peterson, P., Landsfeld, M., Pedreros, D., Verdin, J., Shukla, S., ... & Husak, G. (2015). The climate hazards infrared precipitation with stations—a new environmental record for monitoring extremes. *Scientific Data, 2*: 150066. https://doi.org/10.1038/sdata.2015.66

Horritt, M.S., & Bates, P.D. (2002). Evaluation of 1D and 2D numerical models for predicting river flood inundation. *Journal of Hydrology*, 268(1–4): 87–99 https://doi.org/10.1016/S0022-1694(02)00121-X

Jonkman, S.N., & Kelman, I. (2005). An analysis of the causes and circumstances of flood disaster deaths. *Disasters*, 29(1): 75–97. https://doi.org/10.1111/j.0361-3666.2005.00275.x

Kefi, A.S., Mutua, F., & Shisanya, C.A. (2019). Assessment of urban flood impacts on transport and accessibility in Nairobi City County. *Hydrology*, 6(1):6. https://doi.org/10.3390/hydrology6010006

Merz, B., Kreibich, H., Schwarze, R., & Thieken, A. (2007). Review article "Assessment of economic flood damage". *Natural Hazards and Earth System Sciences*, 7(5): 621–633. https://doi.org/10.5194/nhess-7-621-2007

NASA Jet Propulsion Laboratory. (n.d.). *NASA SRTM Global 30m DEM* [Data set]. Google Earth Engine. https://developers.google.com/earth-engine/datasets/catalog/USGS_SRTMGL1_003

Neal, J., Schumann, G., & Bates, P. (2012). A subgrid channel model for simulating river hydraulics and floodplain inundation over large and data sparse areas. *Water Resources Research*: 48(11) https://doi.org/10.1029/2012WR012514

Nicholson, S.E. (2017). Climate and climatic variability of rainfall over Eastern Africa. *Reviews of Geophysics, 55*(3): 590–635 https://doi.org/10.1002/2017RG000562

Novella, N.S., & Thiaw, W.M. (2013). African rainfall climatology version 2 for famine early warning systems. *Journal of Applied Meteorology and Climatology, 52*(3):588–606 https://doi.org/10.1175/JAMC-D-11-0238.1

Nyeko, M. (2021). Flood hazard mapping and vulnerability analysis in Lake Kyoga Basin, Uganda, using remote sensing and hydraulic modeling. *Journal of Flood Risk Management,* 14(3): e12692. https://doi.org/10.1111/jfr3.12692

Onywere, S.M., Majanga, E., & Ndiritu, J.G. (2011). Analysis of the spatial and temporal rainfall characteristics of the Tana River Basin, Kenya. *Journal of Meteorology and Related Sciences*, 5(1): 13–26

Otieno, G., & Anyah, R. (2013). Multi-model ensemble simulations of the East African climate: Analysis of twentieth century simulations and twenty-first century projections using the AR4 CMIP3 models. *Climate Dynamics*, 41: 2455–2477 https://doi.org/10.1007/s00382-012-1523-0

Schumann, G.J.P., Bates, P.D., Horritt, M.S., & Matgen, P. (2009). Progress in integration of remote sensing–derived flood extent and stage data and hydraulic models. *Reviews of Geophysics*, 47(RG4001): 1–20 https://doi.org/10.1029/2008RG000274

Schumann, G.J.P., Andreadis, K.M., Neal, J.C., & Bates, P.D. (2018). Crowdsourced field data to complement remotely sensed observations for improved flood

inundation modeling. *Geophysical Research Letters*, 45(10): 5144–5151 https://doi.org/10.1029/2018GL077527

Soil Conservation Service (SCS). (1986). *Urban hydrology for small watersheds* (Technical Release No. 55). U.S. Department of Agriculture. Retrieved from https://www.nrcs.usda.gov

U.S. Army Corps of Engineers (USACE). (2021). *Hydrologic Modeling System HEC-HMS User's Manual Version 4.12*. Hydrologic Engineering Center, Davis, CA. Retrieved from https://www.hec.usace.army.mil/software/hec-hms/documentation.aspx

UNDRR. (2022). *Global assessment report on disaster risk reduction 2022: Our world at risk– Transforming governance for a resilient future*. United Nations Office for Disaster Risk Reduction. https://www.undrr.org/gar2022-our-world-risk

USACE. (2021). *HEC-HMS Hydrologic Modeling System User's Manual* (Version 4.9). U.S. Army Corps of Engineers, Hydrologic Engineering Center.

Wainwright, C.M., Finney, D.L., Kilavi, M., Black, E., & Marsham, J.H. (2020). Extreme rainfall in East Africa, October 2019–January 2020 and context under future climate change. *Weather*, 75(9): 294–300 https://doi.org/10.1002/wea.3824

Wood, E.F., Sheffield, J., & Pan, M. (2016). Satellite-based hydrologic modeling: Challenges and progress. *Remote Sensing of Environment,* 180: 4–17 https://doi.org/10.1016/j.rse.2016.02.049

World Bank. (2020). *Kenya Climate Risk Profile: Floods*. World Bank Group. Retrieved from https://climateknowledgeportal.worldbank.org